JACS
JOURNAL OF THE AMERICAN CHEMICAL SOCIETY

COMMUNICATION

pubs.acs.org/JACS

Controlled Nucleation from Solution Using Polymer Microgels

Ying Diao,[†] Matthew E. Helgeson,[†] Allan S. Myerson, T. Alan Hatton, Patrick S. Doyle, and Bernhardt L. Trout*

Novartis-MIT Center for Continuous Manufacturing and Department of Chemical Engineering, Massachusetts Institute of Technology, 77 Massachusetts Avenue, E19-502b, Cambridge, Massachusetts 02139, United States

Supporting Information

ABSTRACT: Despite its widespread occurrence in nature and broad application in industrial practice, nucleation of crystalline materials remains largely unpredictable and therefore difficult to control. In this work, we demonstrate a new method to control nucleation with polymer microgels by tuning their microstructure to vary systematically the degree of nanoscopic confinement and its effects on nucleation. We find that the polymer microstructure has a significant impact on nucleation kinetics. Moreover, there exists an optimum polymer mesh size at which the rate of nucleation is dramatically enhanced, the degree to which depends on the extent of polymer−solute interactions. With easily tunable microstructure and chemistry, polymer microgels offer a promising approach for the rational design of materials for controlling nucleation from solution.

Crystallization from solution is used extensively in the chemical and pharmaceutical industries. However, control of nucleation, the initial step of the crystallization process, remains a major challenge, since the nucleation barrier is extraordinarily sensitive to experimental conditions[1] and various properties of interfaces present in the system,[2] the effects of which are yet to be elucidated on a fundamental level. Furthermore, nucleation of organic molecules from solution presents added complexities stemming from relatively weak intermolecular interactions, flexible molecular conformations[3] and the effect of solvent on molecular processes.

For organic systems, nanoscopic confinement has been utilized to control nucleation kinetics and polymorphic outcome. Recent studies have shown that mesoporous silica with 5−10 nm pores induced protein crystallization from aqueous solution.[4,5] A Monte Carlo (MC) simulation of nucleation for a one component system in a square shaped open pore indicated the existence of an optimum pore size corresponding to a maximal nucleation rate.[6] However, this hypothesis has not been directly verified by experiments. Moreover, the effect of interaction between the crystallizing species and the confining wall on nucleation was largely neglected. Recently, however, Maheshwari and co-workers clearly demonstrated the importance of fluid−wall interactions in dictating the freezing behavior of nanoconfined liquids.[7] Currently, mechanistic understanding of nucleation from solution under nanoconfinement remains inadequate, and thus, systematic studies are necessary to elucidate the effects of confinement and the interfacial interactions on nucleation.

In contrast to rigid materials with nanoscopic pores used in most previous studies (e.g., controlled pore glass,[8] mesoporous silicon,[4] and zeolites[7]), we have employed cross-linked polymer microparticles or "microgels", whose structure is governed by a meshlike network, to study and control heterogeneous nucleation of organic molecules. The cross-linked polymers exhibit a number of promising characteristics. First, their mesh structure can be easily manipulated through synthesis conditions, yielding direct control over the degree of nanoscopic confinement. Second, fluid−polymer interactions can be tuned through the choice of polymer chemistry. These attractive properties enabled us to investigate systematically the role of molecular confinement and interfacial interactions on heterogeneous nucleation.

We synthesized a series of microgels comprised of cross-linked polyethylene glycol diacrylate (PEG_MDA) from PEG_MDA precursors of different average PEG molecular weight, M_n. Specifically, stop flow lithography (SFL)[9] was used to prepare cubelike PEG_MDA microgels (with approximate dimensions of 30 μm × 30 μm × 25 μm) to study heterogeneous nucleation (Figure 1a). The hydrogel precursor consisted of 25% PEG_MDA, 25% polyethylene glycol (M_n = 200 g/mol), and 5% photoinitiator in ethanol. The particles were purified in 38/62 (v/v) ethanol/water, resulting in a kinetically stable dispersion of PEG_MDA hydrogel cubes (Figure 1b). The use of SFL allows for synthesis of highly monodisperse, nonspherical particles whose faces are easily distinguished by optical microscopy. The monodispersity is also ideally suited to isolate the effects of polymer microstructure on heterogeneous nucleation.

Particles were prepared from a series of PEG_MDA monomers with molecular weight M_n ranging from 130 to 700 g/mol, resulting in microgels with a range of interior mesh structures with differing cross-link density. The structure of the cross-linked hydrogel mesh is typically described by the so-called "mesh size", which is related to the average molecular weight between cross-links within the polymer network.[10] In order to determine the changes in hydrogel microstructure between particles of different PEG_MDA molecular weight, equilibrium swelling measurements were used to estimate the apparent mesh size, ξ. Specifically, ξ was computed by the Flory−Rehner theory[11] from the swelling ratio of particles measured in 38/62 (v/v) ethanol/water relative to the as-prepared particles, using literature values of model parameters for PEG_MDA.[12] The resulting estimates of ξ (Figure 1c) show that the mesh size varies nearly linearly with PEG_MDA molecular weight from 0.7 to 2.0 nm over the range studied, which is consistent with literature values.[12]

To study the effect of particles with various mesh sizes on nucleation kinetics, aspirin (ASA) and acetaminophen (ACM)

Received: December 10, 2010
Published: February 23, 2011

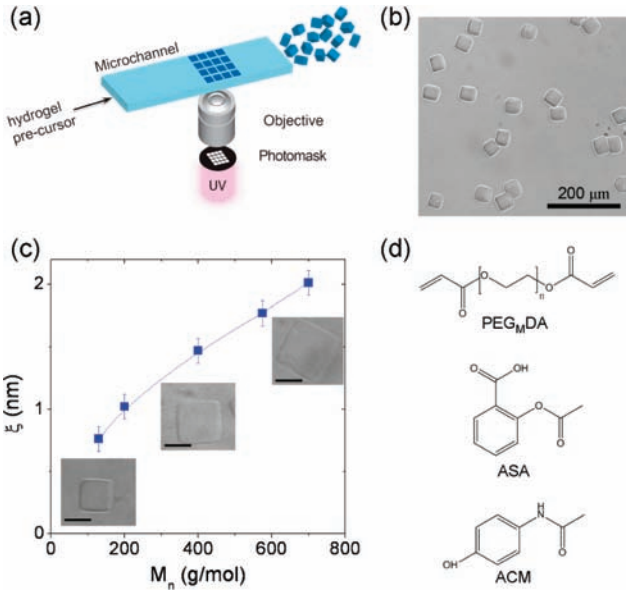

Figure 1. Synthesis and characterization of PEG_MDA microgel particles. (a) Schematic diagram of the SFL process. (b) DIC microscopy image of purified $PEG_{400}DA$ microgel cubes suspended in 38/62 (v/v) ethanol/water. (c) Apparent microgel mesh size versus PEG_MDA molecular weight used in the hydrogel precursor. All measurements are performed in 38/62 (v/v) ethanol/water at 25 °C. (Inset) representative images of swollen particles prepared from respective PEG_MDA molecular weights. Scale bars are 30 μm. (d) Molecular structures of PEG_MDA, aspirin (ASA), acetaminophen (ACM).

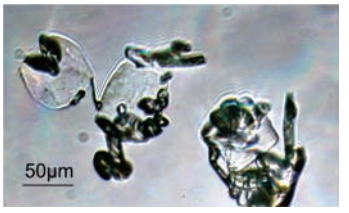

Figure 2. ASA crystals on $PEG_{700}DA$ particles as crystallized from 38 mg/mL ASA solution in 38/62 (v/v) ethanol/water with 15 μg/mL $PEG_{700}DA$ particles at 15 °C, solution stirred at 700 rpm.

were chosen as model compounds, both carrying hydrogen bond donors that could potentially interact with the hydrogen bond acceptors of the polymer mesh. Crystallization of ASA or ACM from its 38/62 (v/v) ethanol/water solution was induced by cooling, with and without PEG_MDA particles suspended in the solution by stirring. Crystallization in the presence of microgels was found to result in the growth of ASA or ACM crystals on or from within the PEG_MDA particles, as observed by optical microscopy (Figure 2). For both systems, the stable polymorph at the crystallization condition was obtained, with or without microgels.

The nucleation kinetics of ASA and ACM templated by PEG_MDA microgels were investigated by measuring the nucleation induction time probability distribution, $P(t)$. The induction time is a useful indicator of the effectiveness of microgels in inducing nucleation because it is highly sensitive to changes in the free energy barrier to nucleation. Due to the stochastic nature of nucleation events, a large number of experiments were performed to obtain the probability distribution of nucleation induction

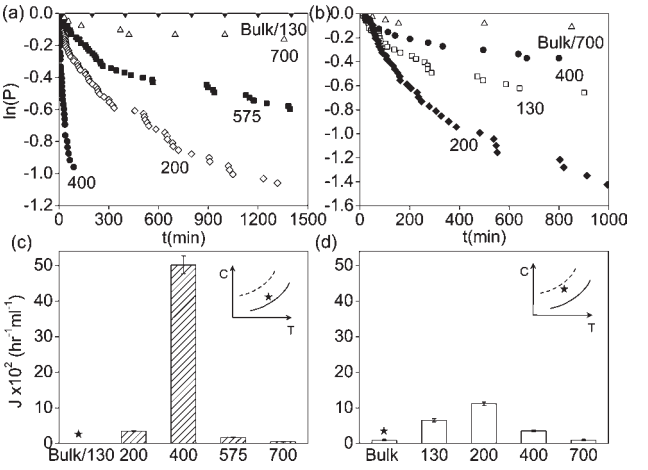

Figure 3. Nucleation kinetics of ASA and ACM with PEG_MDA particles of various M_n. (a, b) Statistical analysis of nucleation induction time for ASA (a) and ACM (b) at supersaturations (S) of 2.1(a) and 3.7(b). The deviation from the Poisson distribution is attributed to limited number of samples and sample variations. (c, d) Nucleation rates of ASA (c) and ACM (d). Nucleation rate J was calculated from the average induction time by $J = 1/\tau V$, where τ is the average induction time, and V is the volume of solution. (Inset) Schematics illustrating the relative position of the bulk solution in the metastable zone under the crystallization conditions. C and T represent the solute concentration and the temperature, respectively.

Table 1. Comparison of ASA Average Nucleation Induction Times (τ) with PEG_MDA Microparticles of Various Mesh Sizes

M_n (g/mol)	130	200	400	575	700
τ (min) $S = 2.1$	>140000	910 ± 40	**63 ± 3**	1900 ± 100	6600 ± 1100
τ (min) $S = 3.4$	330 ± 60	**52 ± 3**	123 ± 7	NA	240 ± 20

ASA crystallization was performed at two supersaturation levels (S), 2.1 and 3.4. The standard errors of average induction times were calculated from the standard error values for the slopes regressed from the ln P vs t plots (Figure 3a,b) following the formula $\ln P = -t/\tau$.

time. The average induction time, τ, was determined from a statistical analysis on the induction time data assuming that nucleation follows a Poisson distribution, $P(t) = \exp(-t/\tau)$.

Figure 3a shows the statistical analysis of ASA nucleation induction time with and without PEG_MDA particles suspended in a supersaturated ASA solution at a particle concentration of 15 μg/mL. The corresponding values of τ are listed in Table 1 (S = 2.1; the supersaturation effect is discussed later). Clearly, almost all particles successfully promoted ASA nucleation, except for those prepared with M_n = 130 g/mol PEG_MDA. Specifically, the addition of particles with M_n = 400 g/mol to the ASA solution dramatically reduced the ASA average nucleation induction time to 63 min, whereas under the same experimental conditions, no nucleation event was detected in the absence of particles. Furthermore, the solute nucleation activity, expressed by the solute nucleation rate, of the PEG_MDA particles decreased sharply for both M_n < 400 g/mol and M_n > 400 g/mol. This observation suggests that there exists an optimum mesh size for accelerating nucleation from solution.

Nucleation induction time measurements on the ACM system (Figure 3b) further demonstrate the overall success of PEG_MDA particles in facilitating nucleation. In most cases, the addition of

dx.doi.org/10.1021/ja110801g |J. Am. Chem. Soc. 2011, 133, 3756–3759

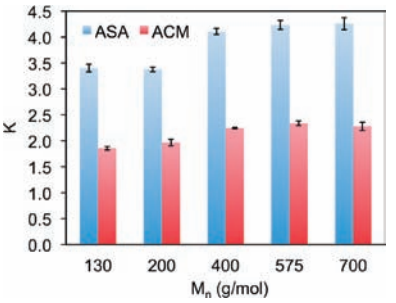

Figure 4. Partition coefficient, κ, of ASA and ACM in the PEG_MDA gel, defined as the ratio of solute concentration in the solution contained in the PEG_MDA gel to that in the bulk.

particles in ACM solution led to a shorter average induction time compared with the bulk. Furthermore, as in the ASA system, an optimum mesh size corresponding to the shortest average nucleation induction time was also observed. However, the effect of PEG_MDA particles was not as dramatic for ACM as in the case of ASA, as evidenced by the following observations. First, the addition of PEG_MDA particles at best resulted in approximately a 10-fold enhancement in the nucleation rate of ACM (Figure 3d), whereas for ASA, the degree of enhancement was by many orders of magnitude (Figure 3c). Second, the particles were unable to induce ACM nucleation at the lower supersaturation levels (S = 2.7, 3.3), within the experimental time frame. At S = 3.7, when the particles began to promote ACM nucleation, the bulk solution started to crystallize at a detectable frequency, implying that this condition was fairly close to the upper bound of the metastable zone (Figure 3d). As for ASA, the PEG_MDA particles showed effects at a much lower supersaturation (S = 2.1). The fact that there was no detectable bulk nucleation under these conditions indicates the solution was far from the boundary of the metastable zone (Figure 3c). These observations suggest that the PEG_MDA particles are less effective in inducing ACM than ASA nucleation.

We hypothesize that the success of PEG_MDA particles in facilitating ASA and ACM nucleation results from favorable interactions between the solute and the PEG_MDA polymer matrix in the solution environment. To prove this hypothesis, we first quantified the partitioning of ASA between the PEG_MDA gel phase and 38/62 (v/v) ethanol/water to determine the actual concentration of ASA in the particles. PEG_MDA gels sufficiently large for convenient handling were synthesized by UV polymerization, following the same formulation as the synthesis of PEG_MDA particles used in the crystallization study. As shown in Figure 4, ASA was concentrated within the PEG_MDA particles by as much as 4-fold with respect to the bulk, while the ethanol concentrations remained comparable to that of the bulk (see Supporting Information). Besides, the partition coefficient for ASA is consistently high for all PEG_MDA molecular weights and remains relatively insensitive to the variation in mesh size. This result indicates that the interaction between ASA molecules and the polymer matrix is favorable as compared to that between ASA and solvent.

Similarly, ACM also interacts favorably with the PEG_MDA matrix, leading to a concentration approximately twice as high as in the bulk (Figure 4), supporting the observation that PEG_MDA particles are generally effective in inducing ACM nucleation. ACM is less concentrated in the PEG_MDA gel phase than ASA (Figure 4), indicating weaker interactions with the PEG_MDA matrix. These observations support the hypothesis that polymer−solute interactions contribute to enhanced nucleation activity, since the PEG_MDA particles are less effective in inducing ACM nucleation than that of ASA.

The results discussed above imply that in addition to their microstructures, the effectiveness of the polymeric particles in promoting nucleation also relies on their interactions with the solute. Furthermore, they indicate that the mechanism of PEG_MDA particle-induced nucleation could be partially explained by the higher solute concentration inside the particles due to the effect of preferential partitioning. However, higher solute concentration in the particles alone is insufficient to facilitate nucleation, considering that particles with M_n = 130 g/mol do not induce ASA nucleation despite a high partition coefficient comparable to that of other particles (likewise for ACM nucleation in the presence of particles with M_n = 700 g/mol). In addition, a higher concentration may not result in a higher supersaturation since the solubility in the swollen microgel may be different from that in the bulk, which will be investigated in the future.

Interestingly, previous studies have shown, contrary to our findings, that strong polymer−fluid or polymer−solute interactions led to the opposite nucleation behavior. Konno and Taylor found that the crystallization of amorphous felodipine was inhibited in polymer−felodipine solid dispersions when the polymers interact with the drug molecule via hydrogen bonding.[13] Vidal et al. also found that nucleation of lysozyme from solution was retarded in silica gels with mesh sizes ranging from 10 nm to 1 μm due to adsorption of protein on the gel surface.[14] An important distinction between our study and the aforementioned studies lies in the microstructure of the polymer present in the crystallization system, among other factors. In addition, our observations that the solute nucleation kinetics are quite sensitive to the polymer mesh size and the existence of an optimum mesh size also imply that the microstructure of the polymer particles plays a crucial role in controlling the nucleation behavior.

The role of gel microstructure in controlling nucleation can be understood in terms of the effects of the polymer mesh on molecular events in solution leading to nucleation. Nucleation of crystalline solids from solution is preceded by the creation of a distribution of molecular clusters via density fluctuation and alignment of molecules within the cluster via structure fluctuation.[15] This cluster formation is governed by effective solute−solute interactions, which are affected by the presence of the polymer mesh via polymer−solute interactions. On one hand, strong polymer−solute interactions lead to higher solute concentration in the polymer gel, which could potentially facilitate solute−solute interactions; on the other hand, it restricts the motion of solute molecules adsorbed to the polymer mesh, and hence, may inhibit solute−solute interactions. This confinement effect manifests itself in solute diffusivities 2−3 orders of magnitude lower in the gel than in the bulk, which we estimated from the solute elution profiles from saturated gels to pure solvent. Given strong polymer−solute interactions and low solute-to-polymer ratios in the gel, it is plausible that most solute molecules are associated with the polymer chain for an extended period of time (Figure 5a), which may inhibit solute−solute interactions necessary for nucleation. However, if the microstructure of the polymer mesh is such that it brings enough absorbed solute molecules to within sufficient proximity, the confinement effect could instead reinforce solute−solute interactions, which helps reduce the barrier to nucleation.

In our study, the optimum mesh size for inducing ASA nucleation was found to be approximately 15 Å, and the diameter of ASA molecules, about 6 Å (estimated from the crystal density).

dx.doi.org/10.1021/ja110801g |*J. Am. Chem. Soc.* 2011, 133, 3756–3759

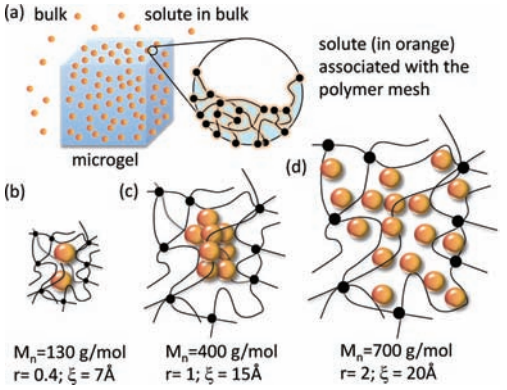

Figure 5. Schematics of nucleation under confinement of a polymer mesh. (a) Polymer mesh in the microgel with concentrated solute molecules. (b−d) Effect of mesh size (ξ) on solute cluster formation. ξ represents the average mesh size of PEG_MDA particles. *r* denotes the molar ratio of ASA to PEG subchain in the gel.

It is probable that the optimum mesh size allows for aspirin molecules associated with polymer chains to come within sufficient proximity to form a nucleus, given the proper orientation (Figure 5c) (as would also be the case with ACM). However, as the mesh size becomes smaller, a solute 'sees' more polymer chains than other solute molecules, which prevents the formation of large enough solute clusters (Figure 5b); for larger mesh sizes, the solutes associated with the polymer chain are further separated from each other; hence, the solute−solute interaction is not enhanced (Figure 5d). On the basis of the above analysis, we hypothesize that the key to controlling nucleation by nanoconfinement lies in manipulating the effective solute−solute interaction, which is strongly affected by polymer−solute interactions and the spatial confinement imposed by the polymer microstructure, the interplay of which gives rise to the observed optimum mesh size for expediting nucleation. To further test this hypothesis, we performed experiments in which the ASA crystallization temperature was lowered from 15 to 8 °C, thereby increasing the supersaturation from 2.1 to 3.4. Since this change in supersaturation is significant while the absolute temperature was only altered by 2%, this experiment primarily probes the effect of increased supersaturation, which should enhance effective solute−solute interactions due to increased density fluctuations. As a result, the observed optimum mesh size decreased from 15 Å to 10 Å at the higher supersaturation level (Table 1). This supports our hypothesis since fewer solute molecules are needed to overcome the nucleation barrier, which is lowered due to higher density fluctuations.

In conclusion, we have demonstrated a new approach to controlling nucleation from solution through the use of polymeric microparticles with tunable microstructure. We found that the nucleation kinetics of aspirin and acetaminophen were very sensitive to variation of the polymer mesh size. Furthermore, an optimum mesh size exists that dramatically enhanced nucleation kinetics, and the overall degree of enhancement was related to the extent of polymer−solute interactions. The uniqueness of employing polymeric microgels to control heterogeneous nucleation from solution is two-fold. First, their microstructure and chemical makeup can be easily tuned over a wide range. Second, their ability to alter the solute concentration in the microgel via thermodynamic partitioning presents an advantage over other types of materials for controlling nucleation. In addition, with PEG-based polymers being biocompatible, these results show promise in a wide range of applications, from designing nucleants for crystallizing small and macro- molecules to enabling multifunctional pharmaceutical excipient and drug-delivery vehicles.

■ ASSOCIATED CONTENT

Supporting Information. Experimental details, including particle synthesis, purification, characterization, and nucleation induction time and partitioning coefficient measurement. This material is available free of charge via the Internet at http://pubs.acs.org

■ AUTHOR INFORMATION

Corresponding Author
trout@mit.edu

Author Contributions
†These authors contributed equally.

■ ACKNOWLEDGMENT

This work was supported by Novartis through the Novartis-MIT Center for Continuous Manufacturing. We also acknowledge Erik Santiso, Manas Shah, Manju Sharma, Lev Bromberg, and Diwakar Shukla for valuable discussions during the course of this investigaton.

■ REFERENCES

(1) Oxtoby, D. W. *Acc. Chem. Res.* **1998**, *31*, 91–97.
(2) Price, C. P.; Grzesiak, A. L.; Matzger, A. J. *J. Am. Chem. Soc.* **2005**, *127*, 5512–5517. Berman, A.; Ahn, D. J.; Lio, A.; Salmeron, M.; Reichert, A.; Charych, D. *Science* **1995**, *269*, 515–518.
(3) Ward, M. D. *Chem. Rev.* **2001**, *101*, 1697–1725.
(4) Chayen, N. E.; Saridakis, E.; El-Bahar, R.; Nemirovsky, Y. *J. Mol. Biol.* **2001**, *312*, 591–595.
(5) Chayen, N. E.; Saridakis, E.; Sear, R. P. *Proc. Natl. Acad. Sci. U.S. A.* **2006**, *103*, 597–601.
(6) Page, A. J.; Sear, R. P. *Phys. Rev. Lett.* **2006**, *97*, 065701/1–065701/4.
(7) Maheshwari, P.; Dutta, D.; Sharma, S. K.; Sudarshan, K.; Pujari, P. K.; Majumder, M.; Pahari, B.; Bandyopadhyay, B.; Ghoshray, K.; Choshray, A. *J. Phys. Chem. C* **2010**, *114*, 4966–4972.
(8) Jackson, C. L.; McKenna, G. B. *Chem. Mater.* **1996**, *8*, 2128–2137. Ha, J. M.; Wolf, J. H.; Hillmyer, M. A.; Ward, M. D. *J. Am. Chem. Soc.* **2004**, *126*, 3382–3383. Beiner, M.; Rengarajan, G. T.; Pankaj, S.; Enke, D.; Steinhart, M. *Nano Lett.* **2007**, *7*, 1381–1385.
(9) Dendukuri, D.; Gu, S. S.; Pregibon, D. C.; Hatton, T. A.; Doyle, P. S. *Lab Chip* **2007**, *7*, 818–828.
(10) Canal, T.; Peppas, N. A. *J. Biomed. Mater. Res.* **1989**, *23*, 1183–1193.
(11) Peppas, N. A.; Hilt, J. Z.; Khademhosseini, A.; Langer, R. *Adv. Mater.* **2006**, *18*, 1345–1360.
(12) Mellott, M. B.; Searcy, K.; Pishko, M. V. *Biomaterials* **2001**, *22*, 929–941.
(13) Konno, H.; Taylor, L. S. *J. Pharm. Sci.* **2006**, *95*, 2692–2705.
(14) Vidal, O.; Robert, M. C.; Boue, F. *J. Cryst. Growth* **1998**, *192*, 271–281.
(15) ten Wolde, P. R.; Frenkel, D. *Science* **1997**, *277*, 1975–1978. Vekilov, P. G. *Cryst. Growth Des.* **2004**, *4*, 671–685. Erdemir, D.; Lee, A. Y.; Myerson, A. S. *Acc. Chem. Res.* **2009**, *42*, 621–629. Santiso, E. E.; Trout, B. L. *J. Chem. Phys.* **2011**. In press.